International Journal of Pharmaceutics 371 (2009) 163–169

Contents lists available at ScienceDirect

International Journal of Pharmaceutics

journal homepage: www.elsevier.com/locate/ijpharm

Pharmaceutical Nanotechnology

SPION-loaded chitosan–linoleic acid nanoparticles to target hepatocytes

Chang-Moon Lee[a,b,c], Hwan-Jeong Jeong[a,b,c,*], Se-Lim Kim[a,b,c], Eun-Mi Kim[a,b,c], Dong Wook Kim[a,b,c], Seok Tae Lim[a,b,c], Kyu Yoon Jang[d], Yong Yeon Jeong[e], Jae-Woon Nah[f], Myung-Hee Sohn[a,b,c]

[a] Biotracer Imaging Laboratory, Chonbuk National University Medical School, Jeonju, Jellabuk-Do 561-712, Republic of Korea
[b] Department of Nuclear Medicine, Chonbuk National University Medical School, Jeonju, Jellabuk-Do 561-712, Republic of Korea
[c] Research Institute of Clinical Medicine, Chonbuk National University Medical School, Jeonju, Jellabuk-Do 561-712, Republic of Korea
[d] Department of Pathology, Chonbuk National University Medical School, Jeonju, Jellabuk-Do 561-712, Republic of Korea
[e] Department of Radiology, Chonnam National University Medical School, Gwangju 501-746, Republic of Korea
[f] Department of Polymer Science and Engineering, Sunchon National University, Jeonnam 540-742, Republic of Korea

ARTICLE INFO

Article history:
Received 19 August 2008
Received in revised form 9 December 2008
Accepted 11 December 2008
Available online 24 December 2008

Keywords:
Hepatocytes
Iron oxide
Superparamagnetic nanoparticle
Chitosan
Linoleic acid
Self-assembled nanoparticle
MRI
Molecular imaging

ABSTRACT

The aim of this study was to develop a novel polymeric magnetic nanoprobe as an MRI contrast agent to target hepatocytes, as well as to evaluate the targeting ability of the nanoprobe with MRI *in vivo*. Superparamagnetic iron oxide nanocrystals (SPIONs) were synthesized by a thermal decomposition and seed growth method. An 1-ethyl-3-(3-(dimethylamino)-propyl) carbodiimide (EDC)-mediated reaction coupled water-soluble chitosan (WSC) to linoleic acid (LA). Twelve-nanometer-sized SPIONs were incorporated into the core of self-assembled WSC–LA nanoparticles. The morphology and size distribution of the SPION-loaded WSC–LA nanoparticles (SCLNs) were determined by transmittance electron microscopy (TEM) and dynamic light scattering (DLS), respectively. The encapsulation of SPIONs in the WSC–LA nanoparticles reduced the cytotoxicity of bare iron particles and enhanced their dispersion ability in water. The clustering of SPIONs into WSC–LA nanoparticles showed ultrasensitive magnetic behavior. After *in vivo* intravascular SCLN injection, MRI revealed relative signal enhancement in the liver. The localization of SCLN in hepatocytes was confirmed by Prussian blue staining and TEM analysis. We have successfully developed an ultrasensitive SCLN that effectively targets hepatocytes. The SCLN can be used as a contrast agent to aid in the diagnosis of hepatic diseases.

1. Introduction

Hepatocyte-selective imaging contrast agents can provide useful information for evaluating hepatic function. For example, liver diseases such as hepatitis reduce the uptake of hepatocyte-targeted imaging agents into hepatocytes (Tanimoto and Kuribayashi, 2005). Other studies have reported that hepatic uptake of a specific imaging agent with hepatocyte affinity reflects hepatic function (Kim et al., 2005, 2006a,b). Therefore, using hepatocyte-targeted contrast agents, hepatic function can be evaluated non-invasively *in vivo*.

Recently, superparamagnetic iron oxide nanocrystals (SPIONs) have been widely studied in biomedical fields such as MRI, magnetic drug delivery, cancer diagnosis and treatment, and biomolecular separation (Kohler et al., 2004). For these applications, SPIONs should be suspended in an aqueous media with comparable stability and have a narrow size distribution (Lutz et al., 2006). To achieve these properties, several polymers such as dextran, poly-ethylene glycol (PEG), alginate, and pullulan have been used for surface modification of SPIONs (Ma et al., 2007; Müller et al., 2007; Gupta and Gupta, 2005; Sun et al., 2006). However, after intravenous injection of SPIONs, most are rapidly cleared from the blood by the reticular endothelial system (RES). The particles then accumulate in several organs such as the liver, spleen, and lymph nodes through the actions of the mononuclear phagocytic system. At the present time, RES-specific contrast agents are used for liver MRI in clinical diagnosis (Karabulut and Elmas, 2006).

In addition to RES-mediated contrast agents, various MRI contrast agents have been developed to target hepatocytes by exploiting the asialoglycoprotein receptor (ASGP-R) on the surface of hepatocytes. Imaging agents bearing β-galactoside and *N*-acetyl-β-galactosaminyl residues are readily recognized by ASGP-R, leading to hepatocyte-specific imaging agents (Jeong et al., 2004). For example, Huang et al. (2008) reported that galactose-terminal SPIONs may function as a targeted imaging agents for ASGPR-expressing cells *in vivo*.

Other ways to target hepatocytes take advantage of biochemical pathways in lipid metabolism. In one pathway, essential polyun-

* Corresponding author at: Department of Nuclear Medicine, Chonbuk National University Hospital, 634-18, Geumam-2 dong, Dukjin-gu, Jeonju City, Jeonbuk 561-712, Republic of Korea. Tel.: +82 63 250 1674; fax: +82 63 250 1676.
E-mail address: jayjeong@chonbuk.ac.kr (H.-J. Jeong).

0378-5173/$ – see front matter © 2008 Elsevier B.V. All rights reserved.
doi:10.1016/j.ijpharm.2008.12.021

saturated fatty acids such as linoleic acid (LA) accumulate in hepatocytes and play a central role in cholesterol and triglyceride synthesis (Giudetti et al., 2005; Ferramosca et al., 2006). For example, Noone et al. (2002) reported that conjugated linoleic acids (CLAs), a mixture of geometrical and positional isomers of LA, reduced very-low-density lipoprotein (VLDL) cholesterol concentrations in healthy humans. Yotsumoto and colleagues also demonstrated that one particular isomer of CLA inhibited cellular cholesterol and triglyceride synthesis in HepG2 cells (Yotsumoto et al., 1999). Most recently, it was suggested that LA-enriched phospholipids act through peroxisome proliferator-activated receptors to stimulate hepatic apolipoprotein A-I secretion in HepG2 cells and human primary hepatocytes (Pandey et al., 2008). This finding supports the hypothesis that LA-based carriers accumulate in hepatocytes. In addition, due to its hydrophobic carbon chain, LA can be used as a hydrophobic segment for self-assembling nanoparticles due to its hydrophobic carbon chain. Therefore, it is conceivable that conjugation of LA to a hydrophilic polymer will results in an amphipathic polymer that not only increases self-assembling capacity but also accumulates in the liver through lipid metabolism.

Self-assembling nanoparticles representare a promising platform for effective drug delivery, gene therapy, and diagnostic imaging (Liang et al., 2006; Park et al., 2007). These nanoparticles are generally composed of copolymers with both hydrophobic and hydrophilic segments. The amphipathic copolymers can self-assemble into core–shell structures of approximately 10–100 nm in diameter in an aqueous solution. The core of the self-assembled nanoparticles provides an effective loading compartment for many hydrophobic drugs, fluorescent probes, and contrast agents, while the shell improves the suspension stability of nanoparticles in an aqueous solution (Park et al., 2006; Nasongkla et al., 2006; Ai et al., 2005). Drugs and imaging probes incorporated into the self-assembled nanoparticles are protected from blood clearance by the RES and thus remain in circulation longer (Torchilin, 2006; Lee et al., 2005). There have been many recent attempts to prepare superparamagnetic self-assembled nanoparticles as an MRI probes (Yang et al., 2007; Okassa et al., 2007; Nakamura et al., 2006).

Chitosan, a natural cationic polysaccharide derived from chitin, has been frequently employed as a polymer for self-assembling nanoparticles, attracting considerable attention in the realms of drug and gene delivery (Jiang et al., 2007; Lee et al., 2006). This compound is also nontoxic, biocompatible, and biodegradable, thus offering powerful potential for biomedical applications. However, natural chitosan is difficult to dissolve in a neutral water solution and is only soluble in an acidic solution, limiting its applications with bioactive materials. Currently, water-soluble chitosan (WSC) is commercially available and has limited biomedical use. Chitosan is composed of D-glucosamine and *N*-acetyl-D-glucosamine linked by β-(1.4)-glycosidic bonds, and thus has free amino and hydroxyl groups. These groups can be modified with hydrophobic segments to improve self-assembling capability by increasing intermolecular hydrophobic interactions between segments (Kim et al., 2006a,b; Liu et al., 2005b).

Consequently, it may be expected that conjugation of LA to chitosan may results in an amphipathic polymer that not only increases has enhanced self-assembling capacity but also accumulates in the liver through lipid metabolism. Moreover, incorporation of Fe_3O_4 into self-assembled nanoparticles could enhance hepatocyte-targeted imaging.

Herein, we report SPION-loaded self-assembled WSC–LA nanoparticles as a hepatocyte-targeting imaging probe with high sensitivity. The WSC–LA amphipathic polymer was designed for the self-assembled nanoparticles to load iron particles. We investigated the nanoprobe's targeted detection ability *in vivo* by MRI.

2. Materials and methods

2.1. Materials

Water-soluble chitosan (WSC, molecular weight: 10 kDa, deacetylation: 97%) was purchased from Kittolife Co. (Seoul, Korea). Linoleic acid, $Fe(acac)_3$ (iron (III) acetylacetonate), oleic acid, oleylamine, 1,2-hexadecanediol, phenyl ether, potassium ferrocyanide (II) trihydrate, nuclear fast red solution, hydroxysuccinimide (NHS), 1-ethyl-3-(3-(dimethylamino)-propyl) carbodiimide (EDC), XTT solution, and paraformaldehyde were purchased from Sigma–Aldrich Chemical Co. (St. Louis, MO). All other chemicals were analytic-grade and used directly without further purification. Female BALB/c mice (5–6 weeks old and weighing 15–18 g), obtained from Orient Bio Inc., were kept in cages and fed standard laboratory chow and water. All animal experiments were approved by the Chonbuk National University Medical School Committee and were performed in accordance with their guidelines.

2.2. Synthesis of WSC–LA conjugates

An EDC-mediated reaction coupled WSC to LA (Liu et al., 2005a,b). Briefly, WSC (100 mg) was dissolved in a solution of distilled water (10 ml) and methanol (8 ml). LA was added to the WSC solution at 0.5 mol/mol. EDC (0.07 g/l) dissolved in 2 ml of methanol was dropped into the solution while stirring at room temperature. After for 24 h, WSC–LA conjugates were precipitated by adding 20 ml of methanol/water (7/3, v/v). The precipitated material was washed with a solution of distilled water, methanol, and ether three times. The final product was purified using dialysis against the mixture of methanol and distilled water (7/3, v/v) and lyophilized. The conjugates were confirmed by ^{1}H NMR analysis.

2.3. Synthesis of SPIONs

We synthesized and used the SPIONs with 12 nm diameter because the bigger iron oxide nanoparticles increase the signal intensity in MRI. Twelve-nanometer SPIONs were synthesized by a two-step procedure. Seed SPIONs were first synthesized by a slight modification of thermal decomposition. Twelve-nanometer nanocrystals were obtained from the seed SPIONs by a seed growth method. To synthesize 4-nm nanocrystals, $Fe(acac)_3$ (2 mmol), 1,2-hexadecanediol (10 mmol), oleic acid (6 mmol), and oleylamine (6 mmol) were dissolved in 20 ml of phenyl ether, magnetically stirred under nitrogen at room temperature, then heated to reflux (265 °C) for 30 min. The resulting solution turned brownish-black and was cooled to room temperature. Black material was precipitated by addition of ethanol and separated by centrifugation. Twelve-nanometer SPIONs were synthesized using 4-nm nanocrystal seeds as described previously (Sun et al., 2004).

2.4. Preparation and characterization of SCLNs

WSC–LA conjugates (50 mg) were dissolved in 5 ml of phosphate-buffered saline (PBS) buffer (0.1 M, pH 7.4) and sonicated for 5 min at 4 °C. We added 0.5 ml of 12 nm SPION solution (1 mg/ml) in chloroform to the WSC–LA solution and sonicated the mixture for 10 min in an ice-water bath. To completely evaporate the organic solvent, the resulting solution was stirred for 12 h at room temperature. The SCLNs were filtered using a syringe filter (0.5 μm pore size) before use in experiments. The morphology of the SCLNs was determined by transmittance electron microscopy (TEM) using an H-7650 electron microscope (Hitachi Ltd., Tokyo, Japan). The size distribution of the SCLNs in distilled water was

analyzed by dynamic light scattering (DLS) using a Microtrac UPA-150 particle size analyzer (Microtrac Inc., Jeonju, KBSI). Incorporated iron was determined according to a previously reported method (Cengelli et al., 2006). SCLN solution was added to 6N HCl (125 μl/well in a 48-well plate). After incubation for 1 h, 5% (w/v) $K_4[Fe(CN)_6]\cdot 3H_2O$ solution was added and the absorbance was read at 690 nm in a multiwall plate reader. $FeCl_3\cdot 6H_2O$ aqueous solution was used as a standard material to quantify the amount of iron. SPIONs loading efficiency was calculated according to the following equation:

$$\text{SPIONs loading efficiency (\%)} = \left(\frac{\text{amount of loaded SPIONs in SCLNs}}{\text{initial feeding amount of SPIONs}}\right) \times 100$$

2.5. Relaxivity measurement of SCLN

T_2 relaxivity of the SCLN was measured using a clinical 1.5 T MRI scanner (GE Signa Exite Twin-speed, GE Health Care, Milwaukee, WI) at room temperature. For the relaxivity measurement, the T_2-weigthed scans were performed with 2400 ms of repetition time (TR) and echo time (TE) ranging from 20 to 200 ms. Relaxivity values were calculated through the least-squares curve fitting of relaxation time versus iron concentration.

2.6. In vitro cytotoxicity assay

To investigate the cytotoxicity of SCLN, an 2,3-bis(2-methoxy-4-nitro-5-sulfophenyl)-2H-tetrazolium hydroxide (XTT) assay was performed. Primary hepatocytes separated from mice were seeded in 96-well plates at a density of 1×10^4 cells/well in 100 μl of medium and incubated overnight at 37 °C. A medium containing varying amounts of nanoparticles was added to the wells. After incubation for 24 or 48 h, the medium was removed by aspiration and the cells were washed with fresh PBS. XTT solution was added to each well. The viability of the cells was determined by measuring absorption at 450 nm on a plate reader.

2.7. MRI

MRI was performed using a 1.5 T clinical MR scanner with an animal coil (4.3 cm quadrature volume coil, Nova Medical System, Wilmington, DE). After anesthetization of mice with 1.5% isoflurane in a 1:2 mixture of O_2/N_2, SCLNs (200 μg of iron per mouse) were injected intravenously through the tail vein. Fast spin echo T_2-weighted images of the mice livers were obtained at 30 min, 1 h, and 2 h with the following parameters: TR = 4200 ms, TE = 102 ms, flip angle of 90°, echo train length of 10, 5-cm field of view, 2-mm section thickness, 0.2 mm intersection gap, 256 × 160 matrix. One radiologist performed the quantitative analysis of the MRIs. The signal intensity (SI) of regions of interest (ROI) in the liver was measured and compared with the back muscle adjacent to the liver. Relative signal enhancement was calculated by SI values before (SI pre) and after (SI post) injection of the SCLNs per the following formula: [(SI post − SI pre)/SI pre]. To verify SCLN localization in hepatocytes, Prussian blue staining and BioTEM analysis were performed.

3. Results

3.1. Synthesis and characterization of WSC–LA conjugates

As shown in Fig. 1, the coupling between WSC (10 kDa) and LA was performed using the EDC-mediated reaction and was confirmed by ^{1}H NMR analysis (Fig. 2). The proton assignment of WSC–LA conjugate is as follows: $\delta_{1.3} = CH_3$ (methyl group of LA); $\delta_{2.0} = CH_3$ (acetyl group of WSC); $\delta_{3.5-4.0} = CH$ (carbon of WSC). The degree of substitution (DS) was calculated by comparing the ratio of methyl protons of LA to sugar protons (Liu et al., 2005a). The number of LA groups per 100 anhydroglucose units of WSC was 43.7. The WSC–LA conjugates were able to form self-assembled nanoparticles with a core–shell structure; the hydrophobic core was used as a site to load SPIONs.

3.2. Preparation and characterization of SCLNs

Following a method described by Sun et al. (2004), hydrophobic magnetite (Fe_3O_4) nanoparticles capped with oleic acid and oleylamine were synthesized with a thermal decomposition method and the particle diameter was controlled with a seed growth method. TEM showed that the magnetite nanoparticles were mostly spherical and uniform with a narrow distribution (Fig. 3). The mean diameter of the magnetite nanoparticles as determined by dynamic light scattering (DLS) was approximately 11.7 ± 1.5 nm. The magnetite nanoparticles with 12 nm diameters were successfully synthesized from 4-nm particles by a seed growth method. As shown in Scheme 1, hydrophobic SPIONs were loaded into the self-assembled WSC–LA nanoparticles by a sonication and

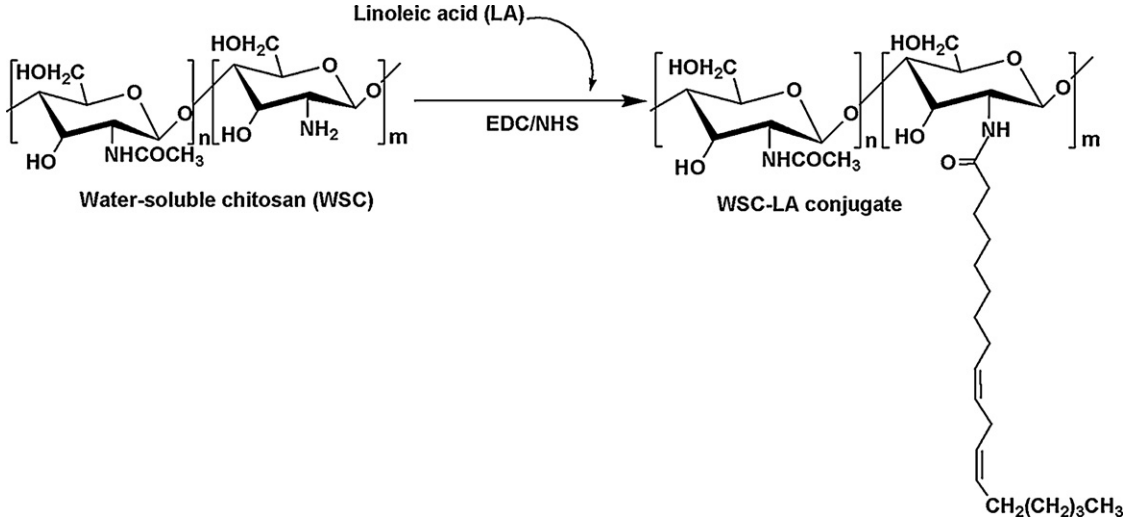

Fig. 1. Schematic illustration of WSC–LA synthesis.

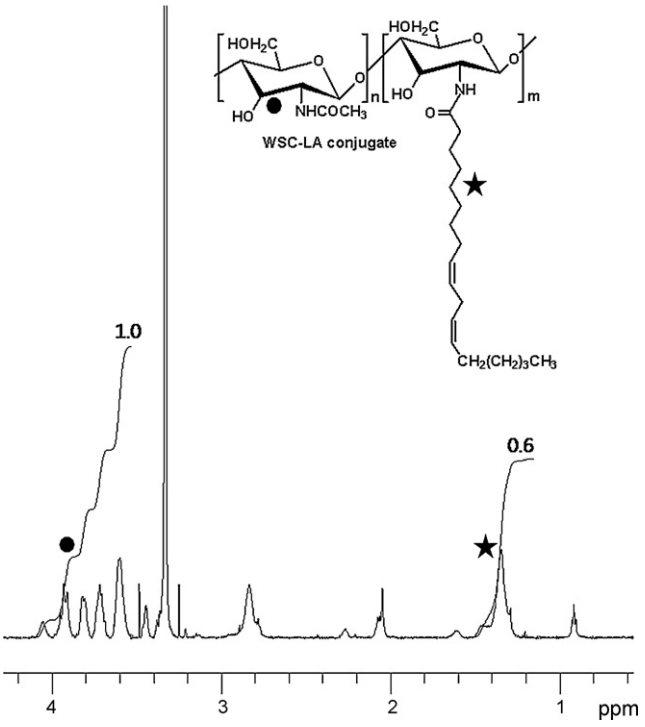

Fig. 2. ^{1}H NMR spectrum of WSC–LA conjugates. The solid circle (●) and star (⋆) correspond to the proton attached to C1-6 of WSC and the proton attached to the methyl group of LA, respectively.

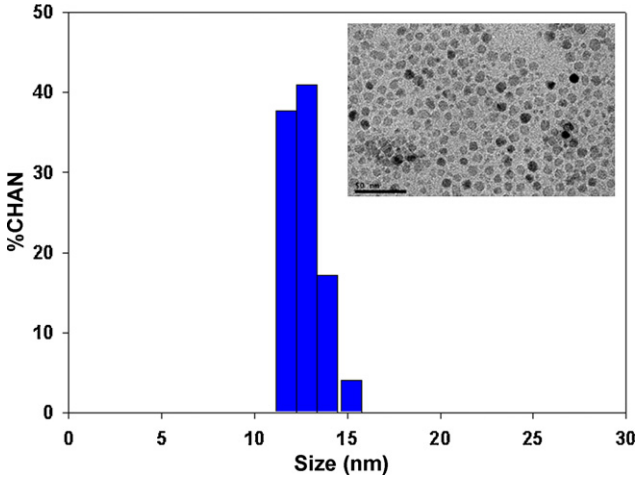

Fig. 3. Size distribution of SPIONs measured by DLS analysis. Inset shows the TEM image of the SPIONs.

solvent-evaporation method (Park et al., 2007). The self-assembled nanoparticle structure for SPION loading allows suspension of SPIONs in aqueous solution without sedimentation. As shown in Fig. 4A, clustering of multiple SPIONs loaded into a single WSC–LA nanoparticle was observed by TEM after negative staining with phosphotungstic acid (PTA). DLS results showed that the mean SCLN diameter was approximately 67 ± 13 nm (Fig. 4B). SPION loading efficiency was $97 \pm 2.8\%$.

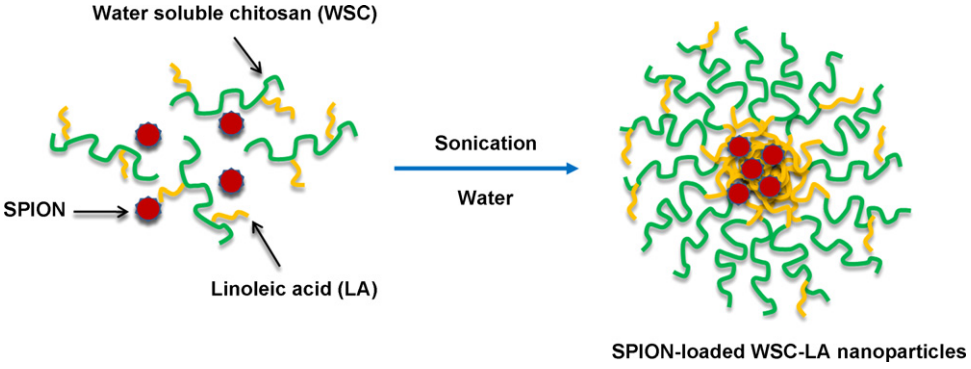

Scheme 1. Schematic illustration for the formation of the SCLN.

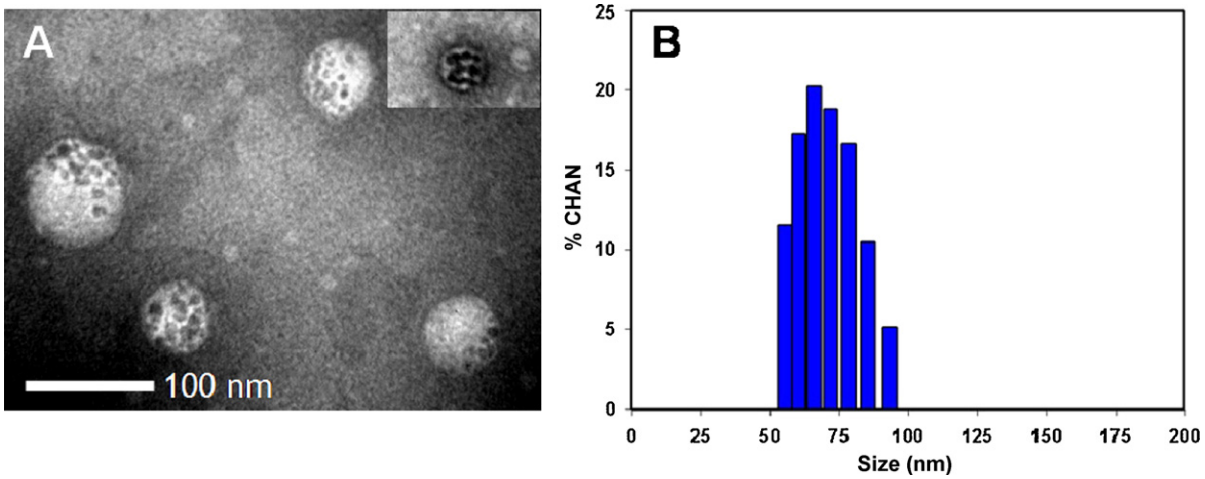

Fig. 4. TEM images of SCLNs with negative staining using phospotungstic acid. Inset shows the TEM image of the same nanoparticles without staining (A). Size distribution of SCLNs as determined by DLS (B).

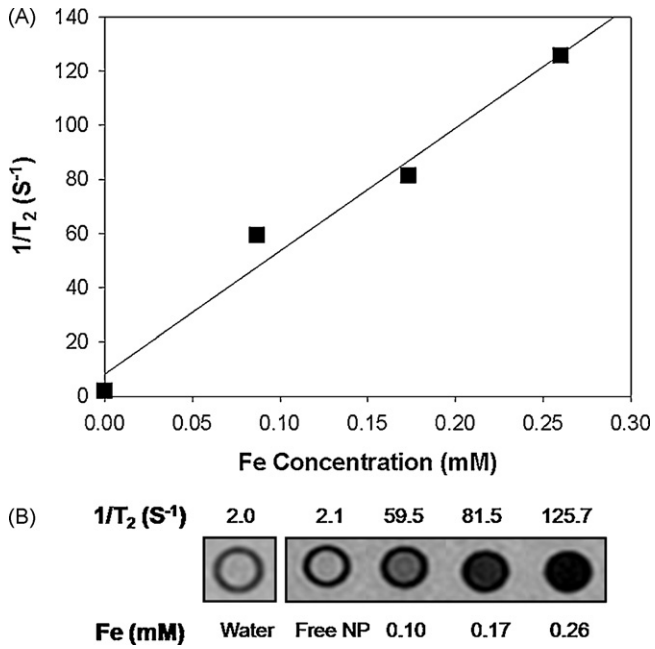

Fig. 5. T_2 relaxation rate ($1/T_2$, S^{-1}) versus iron concentration (mM) in SCLN on a 1.5 T clinical MR scanner (A). T_2-weighted MR images of the same nanoparticles in aqueous solution (B). Free NP indicates WSC–LA nanoparticles without SPION loading.

3.3. MR sensitivity of SCLNs

The T_2 relaxivities of SCLNs in water were measured using a clinical 1.5 T MRI scanner. As shown in Fig. 5, the clustering of SPIONs into the WSC–LA nanoparticles exhibited superparamagnetic behaviors and the T_2 relaxivity was increased dramatically. MRI was also performed to confirm the superparamagnetic effect of the SCLNs. Intensity (darkness) of T_2-weighted MR images of the SCLNs in water solution was increased in a Fe concentration-dependent manner. Solution alone or nanoparticles without SPIONs did not result in any images.

3.4. In vitro cell viability

SCLN cytotoxicity was investigated *in vitro* using an XTT assay. Fig. 6 shows cell viability results for primary hepatocytes after 24 and 48 h of incubation with increasing amounts of SCLNs. SPIONs encapsulated by WSC–LA nanoparticles exhibited little cytotoxicity to the cells at relatively high concentrations. Cells were approximately 73.4% viable with 100 mg/ml of SCLN after incubation for 48 h. The WSC–LA conjugates encapsulating the SPION effectively reduced the cytotoxicity of iron particles.

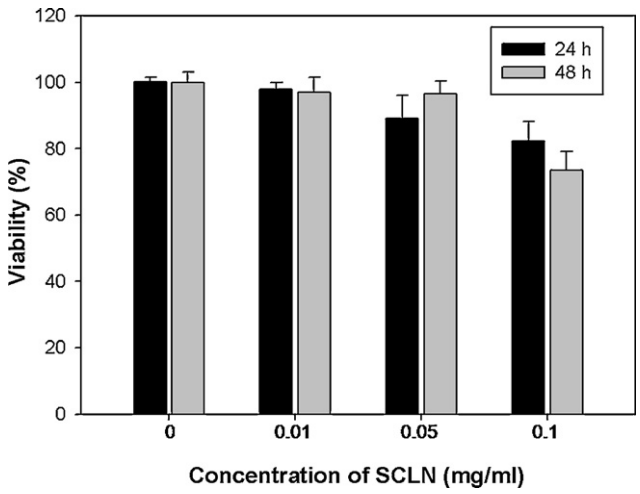

Fig. 6. *In vitro* cell viability of primary hepatocytes treated with SCLNs by XTT assay.

3.5. In vivo MRI

To investigate whether SCLNs can be used as an MRI contrast agent to target hepatocytes, an *in vivo* study was performed using normal mice. The T_2-weighted MR images of the central region of the liver before and after injection of SCLNs via the tail vein are shown in Fig. 7. The signal intensity of T_2-weighted images clearly dropped after injection of SCLNs. The relative signal enhancement of the liver MR images showed a T_2-signal drop of 69.2, 78.2, and 62.9% at 30 min, 1 h, and 2 h after injection of the nanoparticles, respectively. Signal enhancement in the liver with the highest T_2-signal drop was observed 1 h after injection. We also investigated the accumulation of nanoparticles in other organs such as the kidney and spleen. Although we observed no accumulation in the spleen, nanoparticles cleared from the blood through renal excretion appeared in the urine.

3.6. Prussian blue staining and TEM analysis of liver tissue

To confirm SCLN localization in hepatocytes, Prussian blue staining and BioTEM analysis were performed. Fig. 8 shows liver tissue stained with Prussian blue. SCLNs accumulated mainly in the cytoplasm of hepatocytes (Fig. 8A). In contrast, after co-injection of free LA (500 μg per mouse) and SCLNs, nanoparticles were barely observed (Fig. 8B), showing that LA inhibits translocation of SCLNs into the cytosol of hepatocytes. BioTEM analysis revealed compact

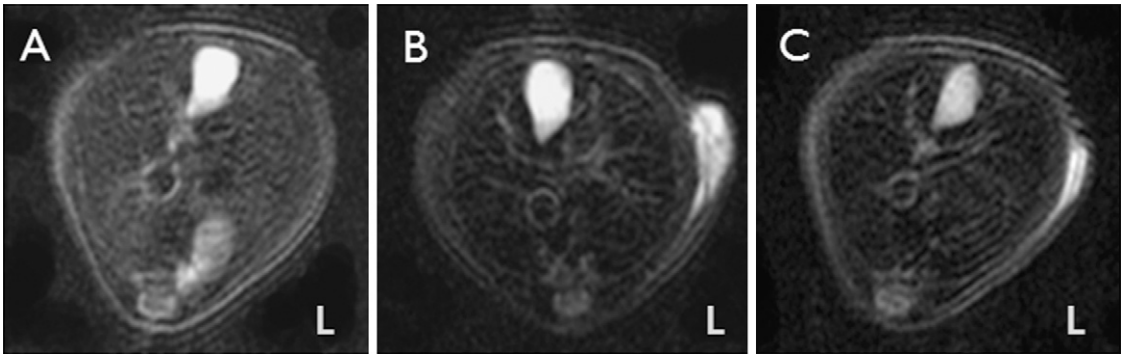

Fig. 7. MRIs of the central region of mice livers before (A) and after (B and C) injection of SCLNs. Images were obtained at (B) 30 min and (C) 1 h after injection of the nanoparticles. L = left.

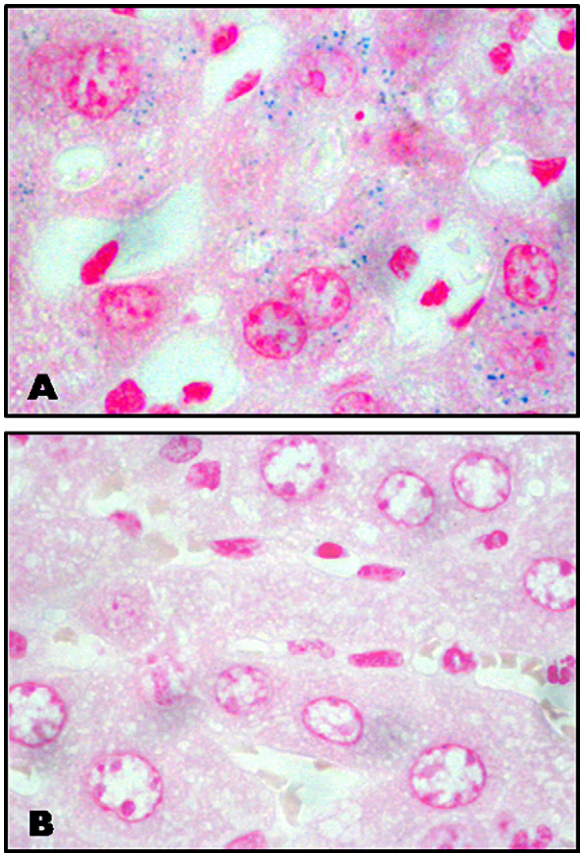

Fig. 8. Photographic images of Prussian blue-stained and nuclear fast red-counterstained liver tissues after injection of SCLNs (A) and co-injection of nanoparticles and LA (B). Magnification = 1000×.

nanoparticles in the cytoplasm of hepatocytes, especially within mitochondria (Fig. 9B). In contrast, no appreciable numbers of particles were found in the mitochondria of hepatocytes without injection of SCLNs (Fig. 9A).

4. Discussion

Various SPION-based contrast agents are available for clinical MRI of the liver (Rappeport and Loft, 2007). However, these agents, such as ferumoxides and ferucarbotaran, are readily taken up by both Kupffer cells in the liver and macrophages in the spleen (Weissleder et al., 1989). In this study, we prepared SCLNs as a specific contrast agent for hepatocyte-targeted imaging to improve the detection of various hepatic diseases. The main advantages of SCLNs are that they (1) accumulate mainly in hepatocytes, thus selective MRI can be performed for hepatocyes not Kupffer cells, (2) have SPION cluster in the WSC–LA nanoparticles, leading an ultrasensitive MR relaxivity, (3) can load a drug into the particle core and deliver to hepatocytes, and (4) can readily form complexes for gene delivery because the surface of SCLNs exhibit positive charge. To develop a hepatocyte-targeted contrast agent, we synthesized WSC–LA conjugates as an amphipathic polymer. The hydrophobic core of the amphipathic WSC–LA conjugates serves as a loading site for SPIONs and LA, which impart the ability to target hepatocytes. The WSC–LA conjugates were able to form self-assembled nanoparticles with a core–shell structure; the WSC–LA nanoparticles containing SPIONs were approximately 67 nm in diameter in aqueous solution. Hattori et al. (2000) demonstrated that the diameter of the fenestrate of the liver sinusoid is usually smaller than 100 nm. Particles with a diameter larger than 200 nm are readily taken up by monocytes and RES (Rieder et al., 1992). Thus, the particle size to reach hepatocytes should be smaller than the diameter of the fenestrate.

Next, we successfully loaded the SPIONs into the core site of the WSC–LA nanoparticles. SPIONs show signal intensity loss in T_2-weighted MRI due to the susceptibility effects of iron. We chose and synthesized 12 nm-sized SPIONs for high T_2 signal intensity. Previous reports confirmed that the larger the nanoparticles, the higher the signal intensity (Jun et al., 2005). The self-assembling nanoparticle structure for SPION loading allows suspension of SPIONs in aqueous solution without sedimentation. Encapsulation of SPIONs inside the self-assembled nanoparticles can also avoid exposure of their hydrophobic surface, thereby preventing adsorption of blood proteins and prolonging circulation time in the blood.

SPION clustering in the WSC–LA nanoparticles drastically increases image contrast as well as T_2 relaxivity. SPIO-dextran particles currently used in clinical diagnosis have a T_2 relaxivity value of 30–50 $mM^{-1}\,S^{-1}$ (Ai et al., 2005). In contrast, SCLN particle relaxivity in a magnet field was 462 $mM^{-1}\,S^{-1}$, almost 10 times higher. These results indicate that WSC–LA nanoparticles containing SPIONs dramatically enhance image contrast, offering a more accurate MRI.

Conventional SPIONs have cytotoxic effects on cells (Gupta and Gupta, 2005). SCLNs, however, showed little toxicity at high iron concentrations. The WSC–LA conjugates encapsulating SPIONs improve the colloidal suspension of the SPIONs in aqueous solution and effectively reduce cytotoxicity. This result demonstrates that SCLNs are a nontoxic contrast agent for MRI.

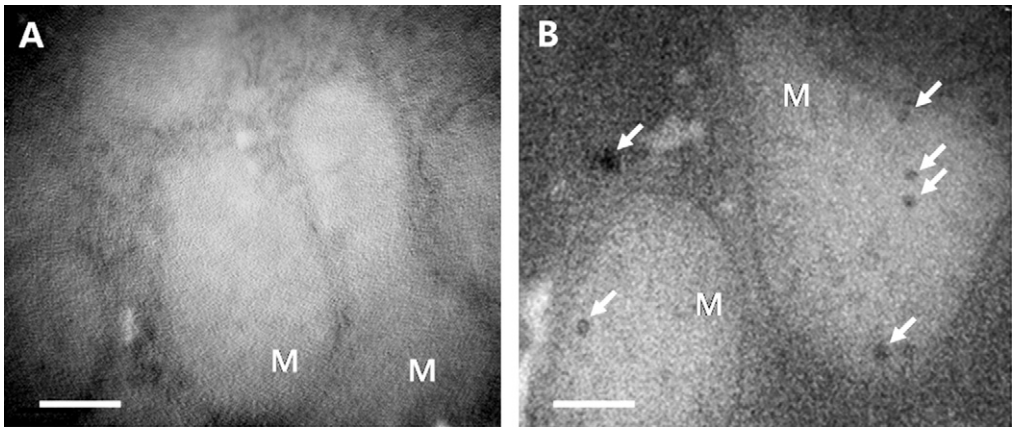

Fig. 9. TEM images of mouse liver tissue before (A) and after (B) injection of SCLNs. The nanoparticles were briefly observed in the mitochondrial matrix of hepatocytes. White arrows indicate SCLNs localized in the mitochondrial matrix. Scale bars are 200 nm. M = mitochondria.

In *in vivo* MRI studies, SCLNs effectively lowered the signal intensity of liver MR images. To investigate SCLN accumulation in hepatocytes, a Prussian blue stain was performed, which showed accumulation of these particles in the cytosol of hepatocytes. Furthermore, the *in vivo* competition study with free LA revealed that translocation of the SCLNs into hepatocytes occurs with the assistance of LA (Fig. 8). TEM confirmed the hepatocyte localization of SCLNs (Fig. 9). One possible mechanism for this localization could be that the SCLNs are driven into hepatocytes by LA conjugated to chitosan during hepatic lipid metabolism (Giudetti et al., 2005).

In summary, we have developed novel self-assembling nanoparticles composed of amphipathic WSC–LA conjugates for encapsulation of SPIONs as a contrast agent to target hepatocytes. The WSC–LA conjugates self-assembled into core–shell structures in aqueous solution. The SPION clusters formed inside the hydrophobic core showed ultrasensitive MRI relaxivity. The SCLNs accumulated mainly in hepatocytes *in vivo*. Thus SCLNs can be used as a contrast agent to investigate hepatic diseases. In future studies, we will evaluate the use of SCLNs as a contrast agent to diagnose the progress of hepatic diseases using a cirrhosis model.

Acknowledgments

This study was supported by a grant of National R&D Program for Cancer Control, Ministry of Health, Welfare and Family affairs, Republic of Korea (0620220 and 0720420).

References

Ai, H., Flask, C., Weinberg, B., Shuai, X., Pagel, M.D., Farrell, D., Duerk, J., Gao, J., 2005. Magnetite-loaded polymeric micelles as ultrasensitive magnetic-resonance probes. Adv. Mater. 17, 1949–1952.

Cengelli, F., Maysinger, D., Tschudi-Monnet, F., Montet, X., Corot, C., Petri-Fink, A., Hofmann, H., Juillerat-Jeanneret, L., 2006. Interaction of functionalized superparamagnetic iron oxide nanoparticle with brain structures. J. Pharmacol. Exp. Ther. 318, 108–116.

Ferramosca, A., Savy, V., Conte, L., Colombo, S., Einerhand, A.W., Zara, V., 2006. Conjugated linoleic acid and hepatic lipogenesis in mouse: role of the mitochondrial citrate carrier. J. Lipid Res. 47, 1994–2003.

Giudetti, A.M., Beynen, A.C., Lemmens, A.G., Gnoni, G.V., Geelen, M.J., 2005. Hepatic lipid and carbohydrate metabolism in rats fed a commercial mixture of conjugated linoleic acids (Clarinol G-80). Eur. J. Nutr. 44, 33–39.

Gupta, A.K., Gupta, M., 2005. Synthesis and surface engineering of iron oxide nanoparticles for biomedical applications. Biomaterials 26, 1565–1573.

Hattori, Y., Kawakami, S., Yamashita, F., Hashida, M., 2000. Controlled biodistribution of galactosylated liposomes and incorporated probucol in hepatocyte-selective drug targeting. J. Control. Release 69, 369–377.

Huang, G., Diakur, J., Xu, Z., Wiebe, Li., 2008. Asialoglycoprotein receptor-targeted superparamagnetic iron oxide nanoparticles. Int. J. Pharm. 360, 197–203.

Jeong, J.M., Hong, M.K., Lee, J., Son, M., So, Y., Lee, D.S., Chung, J.K., Lee, M.C., 2004. ^{99m}Tc-neolactosylated human serum albumin for imaging the hepatic asialoglycoprotein receptor. Bioconjug. Chem. 15, 850–855.

Jiang, H.L., Kwon, J.T., Kim, Y.K., Kim, E.M., Arote, R., Jeong, H.J., Nah, J.W., Choi, Y.J., Akaike, T., Cho, M.H., Cho, C.S., 2007. Galactosylated chitosan-graft-polyethylenimine as a gene carrier for hepatocyte targeting. Gene Ther. 14, 1389–1398.

Jun, Y.W., Huh, Y.M., Choi, J.S., Lee, J.H., Song, H.T., Kim, S., Yoon, S., Kim, K.S., Shin, J.S., Suh, J.S., Cheon, J., 2005. Nanoscale size effect of magnetic nanocrystals and their utilization for cancer diagnosis via magnetic resonance imaging. J. Am. Chem. Soc. 127, 5732–5733.

Karabulut, N., Elmas, N., 2006. Contrast agents used in MR imaging of the liver. Diagn. Interv. Radiol. 12, 22–30.

Kim, D.G., Jeong, Y.I., Choi, C., Roh, S.H., Kang, S.K., Jang, M.K., Nah, J.W., 2006a. Retinol-encapsulated low molecular water-soluble chitosan nanoparticles. Int. J. Pharm. 319, 130–138.

Kim, E.M., Jeong, H.J., Kim, S.L., Sohn, M.H., Nah, J.W., Bom, H.S., Park, I.K., Cho, C.S., 2006b. Asialoglycoprotein-receptor-targeted hepatocyte imaging using ^{99m}Tc-galactosylated chitosan. Nucl. Med. Biol. 33, 529–534.

Kim, E.M., Jeong, H.J., Park, I.K., Cho, C.S., Kim, C.G., Bom, H.S., 2005. Hepatocyte-targeted nuclear imaging using ^{99m}Tc-galactosylated chitosan: conjugation, targeting, and biodistribution. J. Nucl. Med. 46, 141–145.

Kohler, N., Fryxell, G.E., Zhang, M., 2004. A bifunctional poly(ethylene glycol) silane immobilized on metallic oxide-based nanoparticles for conjugation with cell targeting agents. J. Am. Chem. Soc. 126, 7206–7211.

Lee, C.M., Choi, Y., Huh, E.J., Lee, K.Y., Song, H.C., Sun, M.J., Jeong, H.J., Cho, C.S., Bom, H.S., 2005. Polyethylene glycol (PEG) modified ^{99m}Tc-HMPAO-liposome for improving blood circulation and biodistribution: the effect of the extent of PEGylation. Cancer Biother. Radiopharm. 20, 620–628.

Lee, C.M., Heo, Y.J., Song, H.C., Bom, H.S., Lee, H.C., Jeong, H.J., Lee, K.Y., 2006. Radioevaluation of PAMs, CMS, and PS-Lip as an oral carrier for vaccine delivery into intestinal Peyer's patches. Drug Dev. Res. 67, 884–889.

Liang, H.F., Chen, S.C., Chen, M.C., Lee, P.W., Chen, C.T., Sung, H.W., 2006. Paclitaxel-loaded poly(γ-glutamic acid)-poly(lactide) nanoparticles as a targeted drug delivery system against cultured HepG2 cells. Bioconjug. Chem. 17, 291–299.

Liu, C.G., Desai, K.G., Chen, X.G., Park, H.J., 2005a. Linoleic acid-modified chitosan for formation of self-assembled nanoparticles. J. Agric. Food Chem. 53, 437–441.

Liu, C.G., Desai, K.G., Chen, X.G., Park, H.J., 2005b. Preparation and characterization of nanoparticles containing trypsin based on hydrophobically modified chitosan. J. Agric. Food Chem. 53, 1728–1733.

Lutz, J.F., Stiller, S., Hoth, A., Kaufner, L., Pison, U., Cartier, R., 2006. One-pot synthesis of pegylated ultrasmall iron-oxide nanoparticles and their in vivo evaluation as magnetic resonance imaging contrast agents. Biomacromolecules 7, 3132–3138.

Ma, H.L., Qi, X.R., Maitani, Y., Nagai, T., 2007. Preparation and characterization of superparamagnetic iron oxide nanoparticles stabilized by alginate. Int. J. Pharm. 333, 177–186.

Müller, K., Skepper, J.N., Posfai, M., Trivedi, R., Howarth, S., Corot, C., Lancelot, E., Thompson, P.W., Brown, A.P., Gillard, J.H., 2007. Effect of ultrasmall superparamagnetic iron oxide nanoparticles (Ferumoxtran-10) on human monocyte-macrophages in vitro. Biomaterials 28, 1629–1642.

Nakamura, E., Makino, K., Okano, T., Yamamoto, T., Yokoyama, M., 2006. A polymeric micelle MRI contrast agent with changeable relaxivity. J. Control. Release 114, 325–333.

Nasongkla, N., Bey, E., Ren, J., Ai, H., Khemting, C., Guthi, J.S., Chin, S.F., Sherry, A.D., Boothman, D.A., Gao, J., 2006. Multifunctional polymeric micelles as cancer-targeted MRI-ultrasensitive drug delivery systems. Nanoletters 6, 2427–2430.

Noone, E.J., Roche, H.M., Nugent, A.P., Gibney, M., 2002. The effect of dietary supplementation using isomeric blends of conjugated linoleic acid on lipid metabolism in healthy human subjects. J. Br. J. Nutr. 88, 243–251.

Okassa, L.N., Marchais, H., Douziech-Eyrolles, L., Hervé, K., Cohen-Jonathan, S., Munnier, E., Soucé, M., Linassier, C., Dubois, P., Chourpa, I., 2007. Optimization of iron oxide nanoparticles encapsulation within poly(D,L-lactide-co-glycolide) sub-micron particles. Eur. J. Pharm. Biopharm. 67, 31–38.

Pandey, N.R., Renwick, J., Misquith, A., Sokoll, K., Sparks, D.L., 2008. LA-enriched phospholipids act through peroxisome proliferator-activated receptors to stimulate hepatic apolipoprotein A-I secretion. Biochemistry 47, 1579–1587.

Park, K., Kim, J.H., Nam, Y.S., Lee, S., Nam, H.Y., Kim, K., Park, J.H., Kim, I.S., Choi, K., Kim, S.Y., Kwon, I.C., 2007. Effect of polymer molecular weight on the tumor targeting characteristics of self-assembled glycol chitosan nanoparticles. J. Control. Release 122, 305–314.

Park, M.J., Char, K., Park, J., Hyeon, T., 2006. Effect of the casting solvent on the morphology of poly(styrene-*b*-isoprene) diblock copolymer/magnetic nanoparticle mixtures. Langmuir 22, 1375–1378.

Rappeport, E.D., Loft, A., 2007. Liver metastases from colorectal cancer: imaging with superparamagnetic iron oxide (SPIO)-enhanced MR imaging, computed tomography and positron emission tomography. Abdom. Imaging 32, 624–634.

Rieder, H., Meyer zum Buschenfelde, K.H., Ramadori, G., 1992. Functional spectrum of sinusoidal endothelial liver cells: filtration, endocytosis, synthetic capacities and intercellular communication. J. Hepatol. 15, 237–250.

Sun, C., Sze, R., Zhang, M., 2006. Folic acid-PEG conjugated superparamagnetic nanoparticles for targeted cellular uptake and detection by MRI. J. Biomed. Mater. Res. A 78, 550–557.

Sun, S., Zeng, H., Robinson, D.B., Raoux, S., Rice, P.M., Wang, S.X., Li, G., 2004. Monodisperse MFe_2O_4 (M = Fe, Co, Mn) nanoparticles. J. Am. Chem. Soc. 126, 273–279.

Tanimoto, A., Kuribayashi, S., 2005. Hepatocyte-targeted MR contrast enhanced detection of liver cancer in diffusely damaged liver. Magn. Reson. Med. Sci. 4, 53–60.

Torchilin, V.P., 2006. Multifunctional nanocarriers. Adv. Drug Deliv. Rev. 58, 1532–1555.

Weissleder, R., Stark, D.D., Engelstad, B.L., Bacon, B.R., Compton, C.C., White, D.L., Jacobs, P., Lewis, J., 1989. Superparamagnetic iron oxide: pharmacokinetics and toxicity. Am. J. Radiol. 152, 167–173.

Yang, J., Lee, T.I., Lee, J., Lim, E.K., Hyung, W., Lee, H.C., Song, Y.J., Suh, J.S., Yoon, H.G., Huh, Y.M., Haam, S., 2007. Synthesis of ultrasensitive magnetic resonance contrast agents for cancer imaging using PEG-fatty acid. Chem. Mater. 19, 3870–3876.

Yotsumoto, H., Hara, E., Naka, S., Adlof, R.O., Emken, E.A., Yanagita, T., 1999. 10*trans*, 12*cis*-Linoleic acid reduces apolipoprotein B secretion in HepG2 cells. Food Res. Int. 31, 403–409.